BIOLOGICAL CRYSTALLOGRAPHY

ISSN 1399-0047

Structural basis for the catalytic mechanism of homoserine dehydrogenase

Vikas Navratna,[a] Govardhan Reddy[b] and Balasubramanian Gopal[a]*

[a]Molecular Biophysics Unit, Indian Institute of Science, Bangalore, Karnataka 560 012, India, and [b]Solid State and Structural Chemistry Unit, Indian Institute of Science, Bangalore, Karnataka 560 012, India. *Correspondence e-mail: bgopal@mbu.iisc.ernet.in

Received 2 February 2015
Accepted 5 March 2015

Edited by Z. Dauter, Argonne National Laboratory, USA

Keywords: homoserine dehydrogenase; *Staphylococcus aureus*.

PDB references: *S. aureus* homoserine dehydrogenase, 4pg4; 4pg5; 4pg6; 4pg7; 4pg8

Supporting information: this article has supporting information at journals.iucr.org/d

Homoserine dehydrogenase (HSD) is an oxidoreductase in the aspartic acid pathway. This enzyme coordinates a critical branch point of the metabolic pathway that leads to the synthesis of bacterial cell-wall components such as L-lysine and *m*-DAP in addition to other amino acids such as L-threonine, L-methionine and L-isoleucine. Here, a structural rationale for the hydride-transfer step in the reaction mechanism of HSD is reported. The structure of *Staphylococcus aureus* HSD was determined at different pH conditions to understand the basis for the enhanced enzymatic activity at basic pH. An analysis of the crystal structure revealed that Lys105, which is located at the interface of the catalytic and cofactor-binding sites, could mediate the hydride-transfer step of the reaction mechanism. The role of Lys105 was subsequently confirmed by mutational analysis. Put together, these studies reveal the role of conserved water molecules and a lysine residue in hydride transfer between the substrate and the cofactor.

1. Introduction

Homoserine dehydrogenase (HSD; EC 1.1.1.3) is an oxidoreductase that catalyzes the reversible conversion of L-aspartate-β-semialdehyde (ASA) to L-homoserine (L-Hse) in a nucleotide cofactor-dependent reduction reaction (Fig. 1). The L-Hse produced by this enzyme at the first branch point of the aspartic acid pathway is a precursor for essential amino acids such as L-threonine, L-methionine and L-isoleucine. This biochemical pathway also results in dipicolinate and *meso*-diaminopimelic acid (*m*-DAP) synthesis en route to L-lysine. *m*-Diaminopimelic acid and L-lysine are essential components of the peptidoglycan matrix of the bacterial cell wall (Truffa-bachi *et al.*, 1974). In general, HSDs have two domains: a nucleotide cofactor-binding domain and a catalytic domain. The nucleotide cofactor-binding domain has two copies of the characteristic $\beta\alpha\beta\alpha\beta$ (Rossmann) fold. The sequence features and lengths of the β-strands in HSD contribute to structural differences from the lactate dehydrogenase (LDH)-like Rossmann fold. The catalytic domain is comprised of an antiparallel β-sheet that is involved in dimerization and an α-helical cluster that contains the active site (DeLaBarre *et al.*, 2000; Schroeder *et al.*, 2010).

Both bifunctional and monofunctional forms of HSD have been characterized. Monofunctional HSDs are homodimers and are mostly found in fungi, archaea, Gram-positive bacteria and certain Gram-negative bacteria. Bifunctional HSDs (fused to aspartokinase at the N-terminus), on the other hand, adopt a tetrameric arrangement (Archer *et al.*, 1991; Parsot & Cohen, 1988; Schroeder *et al.*, 2010; Thomas *et al.*, 1993). In a

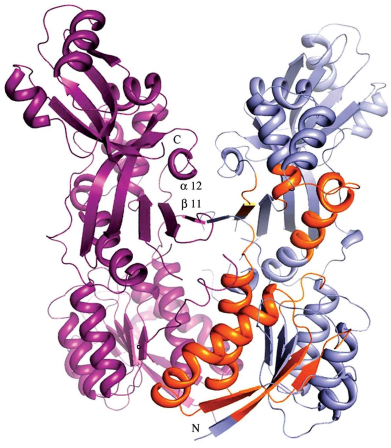

few variants of monofunctional HSDs, primarily from Gram-positive and certain Gram-negative bacteria, the catalytic domain is fused to an additional regulatory domain (ACT domain) at the C-terminus (Curien *et al.*, 2008). The ACT domain [derived from **a**spartokinase, **c**horismate mutase and **T**yrA (prephenate dehydrogenase)], which was first characterized in 3-phosphoglycerate dehydrogenase (3PGDH), is a structurally conserved regulatory module in several enzymes, transcriptional regulators of amino-acid metabolism and some signalling proteins. The ferredoxin-like fold adopted by the ACT domain comprises of a $\beta\alpha\beta\beta\alpha\beta$ unit in which the four β-strands form an antiparallel β-sheet and the two α-helices group together (Aravind & Koonin, 1999). In general, HSDs containing the ACT domain are regulated by feedback inhibition. For example, *Corynebacterium glutamicum* HSD is sensitive to feedback inhibition by L-threonine and mutations in the C-terminal region of the *hom* gene resulted in a feedback-resistant enzyme (Archer *et al.*, 1991, Cremer *et al.*, 1988; Reinscheid *et al.*, 1991). It is also seen that monofunctional HSDs lacking the ACT domain are naturally occurring feedback-resistant forms of this enzyme (Jacques, Nieman *et al.*, 2001).

HSD follows an ordered bi-bi kinetic mechanism, in which NADPH binding precedes the binding of ASA at the active site, whereas the product, L-Hse, is released first followed by $NADP^+$ (Jacques, Ejim *et al.*, 2001; Schroeder *et al.*, 2010). Two probable reaction mechanisms have been proposed for the forward reaction of HSD (DeLaBarre *et al.*, 2000). In one mechanism, the active-site lysine (Lys223 in *Saccharomyces cerevisiae* HSD and Lys205 in the *Staphylococcus aureus* enzyme) donates a proton to the carbonyl O atom at the C4 position of the aldehyde form of ASA, converting it to L-Hse (Fig. 1*a*). The other potential reaction mechanism involves the transfer of a proton from lysine to one of the hydroxyl groups at the C4 position of ASA in the *gem*-diol form. The hydroxyl group is subsequently displaced as a water molecule, generating L-Hse. This reaction mechanism is consistent with the observation that the orientation of L-Hse in the active site in *S. cerevisiae* HSD favours the *gem*-diol form (DeLaBarre *et al.*, 2000; Fig. 1*b*). The proposed reaction mechanism for the reverse reaction catalyzed by HSD involves titration of the catalytic site lysine. It was observed that the catalytic activity of HSD for the conversion of L-Hse to ASA (the reverse reaction) is enhanced at basic pH. This pH dependence on

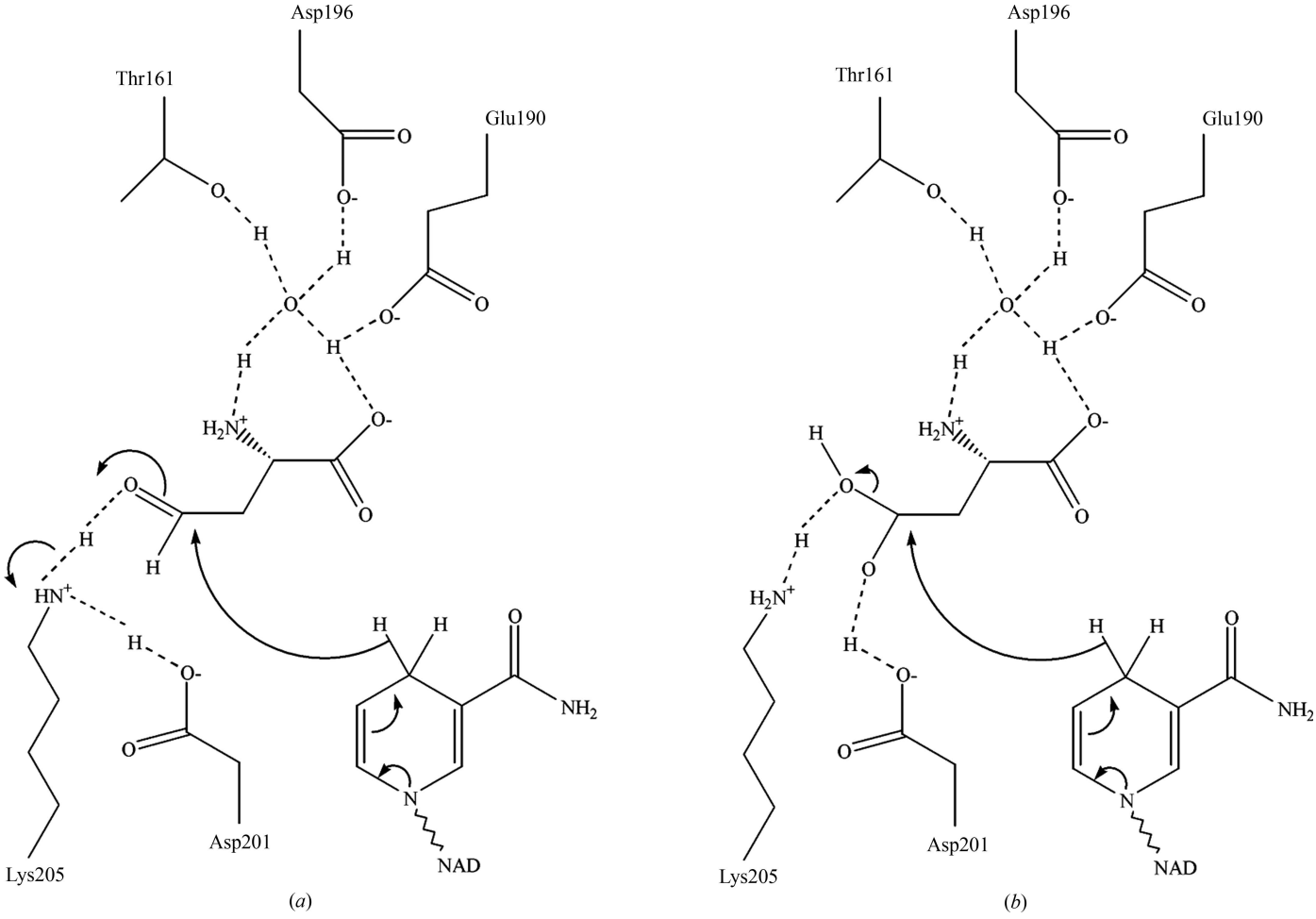

Figure 1
Two potential reaction mechanisms for homoserine dehydrogenase activity. (*a*) The HSD reaction mechanism involving the aldehyde form of ASA. (*b*) A mechanism involving the *gem*-diol form (DeLaBarre *et al.*, 2000). The residue numbering is based on the *S. aureus* enzyme.

Table 1
Data collection and processing.

Values in parentheses are for the outer shell.

pH (PDB code)	pH 8.5 (4pg8)	pH 7.5 (4pg7)	pH 7.0 (4pg6)	pH 6.5 (4pg5)	pH 6.0 (4pg4)
Wavelength (Å)	0.95	0.95	0.95	0.95	0.95
Temperature (K)	100	100	100	100	100
Detector	MAR CCD	MAR CCD	MAR CCD	MAR CCD	MAR CCD
Crystal-to-detector distance (mm)	213.2	263.5	182.1	213.2	213.2
Rotation range per image (°)	0.75	0.75	0.75	0.75	0.75
Space group	$P2_12_12_1$	$P2_12_12_1$	$P2_12_12_1$	$P2_12_12_1$	$P2_12_12_1$
Unit-cell parameters (Å)					
a	72.87	73.04	72.64	72.48	72.46
b	117.51	117.66	116.88	115.43	116.32
c	119.53	119.48	118.62	118.23	118.35
Mosaicity (°)	0.67	0.85	0.56	0.45	0.93
Resolution range (Å)	39.8–2.2 (2.32–2.20)	34.9–2.1 (2.21–2.10)	34.7–2.2 (2.32–2.20)	39.4–2.2 (2.32–2.20)	39.5–2.2 (2.32–2.20)
Total No. of reflections	294024 (42519)	434629 (56962)	433742 (62873)	440608 (62547)	411939 (55716)
No. of unique reflections	52882 (7615)	59396 (8141)	52050 (7494)	51107 (7340)	50394 (6957)
Completeness (%)	99.6 (100.0)	97.8 (93.4)	100.0 (100.0)	100.0 (100.0)	98.0 (94.1)
Multiplicity	5.6 (5.6)	7.3 (7.0)	8.3 (8.4)	8.6 (8.5)	8.2 (8.0)
$\langle I/\sigma(I)\rangle$	15.3 (3.6)	19.2 (4.2)	17.4 (4.7)	20.5 (4.8)	17.0 (4.8)
R_{merge}	0.075 (0.486)	0.057 (0.438)	0.075 (0.442)	0.065 (0.492)	0.071 (0.435)
Overall *B* factor from Wilson plot (Å^2)	33.98	35.83	37.54	38.97	37.64
$CC_{1/2}$	0.99 (0.85)	0.99 (0.92)	0.99 (0.93)	0.99 (0.77)	0.99 (0.95)

Table 2
Structure solution and refinement.

pH (PDB code)	pH 8.5 (4pg8)	pH 7.5 (4pg7)	pH 7.0 (4pg6)	pH 6.5 (4pg5)	pH 6.0 (4pg4)
Resolution range (Å)	39.2–2.2	34.9–2.1	34.7–2.2	38.5–2.2	39.5–2.2
Completeness (%)	100	98	100	100	98
No. of reflections, working set	50125	56338	49330	48454	47777
No. of reflections, test set	2689	2993	2651	2588	2556
Final R_{cryst}	0.201	0.196	0.202	0.201	0.200
Final R_{free}	0.234	0.227	0.244	0.237	0.230
Cruickshank DPI	0.226	0.190	0.190	0.229	0.233
No. of non-H atoms					
Protein	5878	5924	5794	5847	5810
Ligand	95	88	103	87	115
Water	302	321	262	236	255
Total	6275	6333	6199	6170	6180
R.m.s. deviations					
Bonds (Å)	0.010	0.009	0.009	0.010	0.010
Angles (°)	1.3062	1.2688	1.2688	1.3622	1.3706
Average *B* factors (Å^2)					
Overall	41.00	34.50	45.40	48.10	45.40
Protein	40.70	33.70	45.20	48.00	45.10
Ligand	56.80	55.70	61.70	61.80	61.30
Water	41.10	44.90	43.60	45.60	44.70
Ramachandran plot					
Most favoured (%)	98.0	98.0	97.9	97.0	98.0
Allowed (%)	1.6	1.9	1.6	3.0	1.7
Disallowed (%)	0.8	0.1	0.8	0	0.3

catalytic activity has been rationalized to indicate that it is the titration of lysine that facilitates the deprotonation of L-Hse, releasing ASA (Jacques, Ejim *et al.*, 2001). However, the steps involved in the titration of the active-site lysine and proton transfer to the nucleotide cofactor remain unclear. The structure of *S. aureus* HSD provides a rationale for proton transfer between the cofactor-binding and catalytic sites. The structures determined at different pH conditions reveal conserved water molecules, suggesting an important role of hydration dynamics in the reaction mechanism. These findings were subsequently evaluated by mutational analysis.

2. Materials and methods

2.1. Cloning and site-directed mutagenesis of *S. aureus* HSD

The *hom* gene from *S. aureus* spp. COL was PCR-amplified and cloned between the NheI and XhoI restriction sites of the pET-28b and pET-15b expression vectors (Novagen). The K205A, K105A and K105R mutants were generated by a double-primer PCR mutagenesis approach. The parent template was digested with DpnI at 37°C for 3 h following the PCR, and the mutated template was then transformed into *Escherichia coli* DH5α cells. The primers used for cloning are compiled in Supplementary Table S1. The integrity of the clones obtained was confirmed by gene sequencing (Amnion Biosciences).

2.2. Expression and purification of *S. aureus* HSD and mutant enzymes

The plasmids containing *hom* were transformed into *E. coli* Rosetta (DE3) pLysS competent cells. The transformed cells were grown at 37°C to an optical density of 0.5 at 600 nm and overexpression was induced by the addition of 0.4 m*M* isopropyl β-D-1-thiogalactopyranoside (IPTG). Post-induction, the cells were grown at 18°C for 12 h prior to centrifugation at 5000 rev min^{-1} for 15 min. The cells were lysed by sonication after resuspending them in lysis buffer (40 m*M* HEPES pH 7.5, 300 m*M* NaCl, 3% glycerol and EDTA-free protease-inhibitor cocktail tablets). The lysate was centrifuged at 14 000 rev min^{-1} for 40 min at 4°C and the resultant supernatant was incubated with Co^{2+}–NTA affinity beads (Sigma–

Aldrich) for 90 min at 4°C on an end-to-end rotator. The histidine-tagged recombinant protein was eluted using an imidazole gradient (0–300 m*M*) prepared in 40 m*M* HEPES pH 7.5, 300 m*M* NaCl, 3% glycerol. 5 ml of the protein sample (6 mg ml^{-1}) was loaded onto a HiPrep 25/10 desalting column (GE Biosciences) pre-equilibrated with 40 m*M* HEPES pH 7.5, 300 m*M* NaCl, 3% glycerol. The purity of the desalted protein was analyzed by SDS–PAGE and mass spectrometry (Navratna & Gopal, 2013). The K205A, K105A and K105R mutants were purified using the same protocol. The integrity of the mutant proteins was confirmed by mass spectrometry.

2.3. Quaternary-structure analysis of HSD

The quaternary association of HSD and its mutants in solution was determined by analytical size-exclusion chromatography, in which 200 µg (∼1 mg ml^{-1}) purified protein was analyzed at a flow rate of 0.4 ml min^{-1} on a Superdex S200 (10/300 GL) column (GE Biosciences) pre-equilibrated with 40 m*M* HEPES pH 7.5, 300 m*M* NaCl (Supplementary Fig. S1).

2.4. Assay to evaluate cofactor binding

The binding of the nicotinamide cofactor to HSD and its mutants was examined by thermal shift measurements using differential scanning fluorimetry. In these experiments, the reaction mixture consisted of 25 µl 2 µ*M* HSD in 10 m*M* HEPES, 25 m*M* NaCl pH 7.5, 1.5× SYPRO Orange fluorescent dye. The assays were performed in a 96-well iCycler iQPCR plate on a Bio-Rad iCycler iQ5 system. The reaction mixture dispensed into PCR plates was mixed well and subsequently centrifuged at 2000 rev min^{-1} for 10 s. The plate was then sealed with optical quality sealing tape (Bio-Rad). The samples were heated from 20 to 80°C with an increment in temperature of 0.5°C per step and a dwell time of 30 s per step. The fluorescence emitted by SYPRO Orange (excitation maximum at 490 nm; emission maximum at 575 nm) from each well of the plate was recorded at every step of temperature change. The fluorescence intensity was plotted as a function of

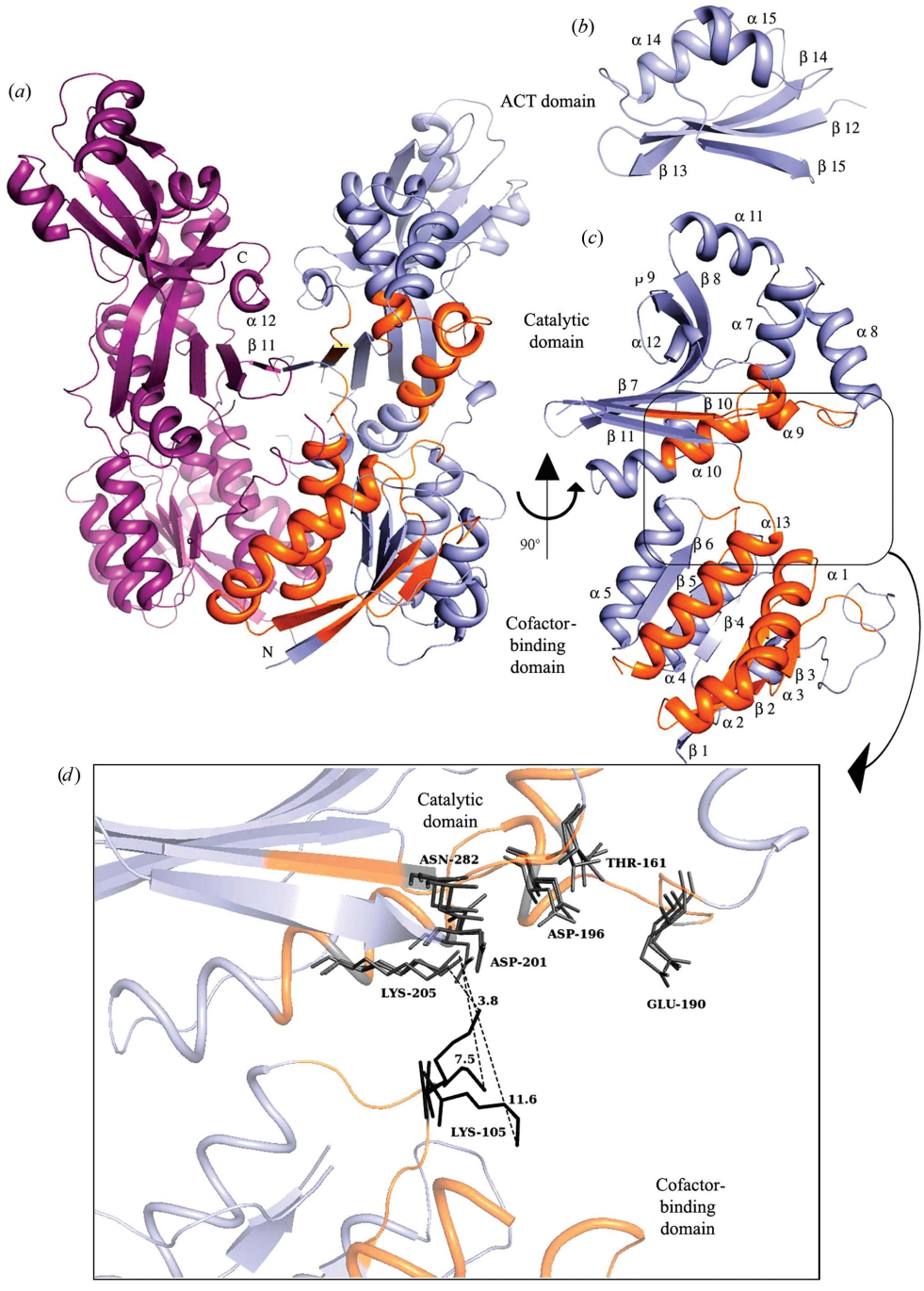

Figure 2
Structural features of *S. aureus* HSD. (*a*) Crystal structure of dimeric *S. aureus* HSD. The two protomers are coloured differently (purple, chain *A*; blue, chain *B*). (*b*) The ACT domain at the C-terminus adopts a ferredoxin-like $\beta\alpha\beta\beta\alpha\beta$ fold. (*c*) The catalytic domain comprises of an antiparallel β-sheet and a α-helical cluster containing the active site (orange). α12 and β11 of the catalytic domain play a major role in dimerization. The nucleotide cofactor-binding domain (α13 is highlighted in orange) adopts a fold that is a variant of the canonical Rossmann fold. (*d*) Residues at the interface between the catalytic and nucleotide-binding domains govern the catalytic mechanism. An important component of this involves hydride transfer governed by Lys105 (structurally characterized alternate conformations are shown).

temperature and fitted to the Boltzmann equation using sigmoidal four-parameter curve fitting in *SigmaPlot* (Systat Software). The assays were performed in the presence of 2 m*M* $NADP^+$ and the changes in T_m were calculated.

2.5. Crystallization, data collection and structure determination

The recombinant protein obtained using the pET-28b expression vector (with polyhistidine tags at both the N- and C-termini) yielded microcrystals in several conditions containing calcium or magnesium salts. However, the recombinant protein obtained using the pET-15b expression vector (with a polyhistidine tag at the N-terminus) yielded better diffracting crystals (Navratna & Gopal, 2013). The initial data were collected on a crystal from a condition consisting of 0.2 *M* magnesium acetate tetrahydrate, 0.1 *M* Tris–HCl pH 7.5, 18%(*w*/*v*) PEG 8000, 5% glycerol. The protein was subsequently crystallized in five different pH conditions (pH 6.0–8.5; Supplementary Table S2). The crystals appeared in a similar time frame across these conditions.

The crystals were flash-cooled in a cryoprotectant consisting of 15% DMSO prepared in the mother-liquor solution and diffraction data were collected on beamline BM14 at the European Synchrotron Radiation Facility (ESRF), Grenoble, France. The data were integrated using *iMosflm* (Battye *et al.*, 2011) and scaled using *SCALA* (Winn *et al.*, 2011). The initial phase information was obtained by molecular replacement (MR) using *Phaser* (McCoy *et al.*, 2007). A putative homoserine dehydrogenase from *Archaeoglobus fulgidus* (PDB entry 3do5; Joint Center for Structural Genomics, unpublished work) was used as a search model in the MR calculations. An edited search model with the catalytic and cofactor-binding domains resulted in a solution with two copies of both the catalytic domain and the NADP-binding domain in the asymmetric unit. The model was rebuilt using *Buccaneer* (Cowtan, 2006) and *Coot* (Emsley & Cowtan, 2004) and was refined using *REFMAC*5 (Murshudov *et al.*, 2011) with TLS groups defined based on analyses from the *TLSMD* server (Painter & Merritt, 2006). The diffraction data and refinement statistics are compiled in Tables 1 and 2.

2.6. Characterization of the enzymatic activity of HSD

The enzymatic activity of *S. aureus* HSD was evaluated using previously described protocols (Schroeder *et al.*, 2010). Briefly, 100 µl of the reaction mixture contained 30 m*M* L-homoserine (Sigma–Aldrich) and varying concentrations of the co-substrate $NADP^+$ (Hi-Media Inc.). HSD was added such that the final concentration of the enzyme in the reaction mixture was 4.5 µ*M*. The reaction mixture was subsequently incubated at 37°C for 45 min and the absorbance at 340 nm was recorded on a Jasco V-630 spectrophotometer. The molar extinction coefficient of $NADP^+$ used in the calculation of the kinetic parameters was 6500 M^{-1} cm^{-1}. The enzyme activity of the K205A, K105A and K105R mutants of *S. aureus* HSD was evaluated using the same protocol. The kinetic behaviour of HSD was also examined in the presence of L-threonine and L-serine (plausible allosteric inhibitors) as well as at different pH values and temperatures. HSD was dialyzed against buffers at different pH conditions (6.5, 7.5, 8.5 and 9.5) and variations in the kinetic parameters were recorded. The effect of metal ions on the activity of HSD was evaluated by performing the assay at 37°C with protein pre-incubated with 5 m*M* metal-salt solutions (Zn^{2+}, Mg^{2+}, Cs^+, Rb^+, Na^+, K^+ and Li^+) for 2 h at 4°C.

2.7. Docking studies

The cofactor-binding site and catalytic site were docked with the cofactor (NADP) and L-homoserine, respectively. The interactions of ligands with HSD were examined *in silico* using a Lamarckian genetic algorithm (LGA) module in *AutoDock* v.4.0 (http://www.autodock.scripps.edu/; Morris *et al.*, 2009). The torsional restraints and internal degrees of freedom were defined using the ligand torsion option and the charges that were assigned to the ligand molecule were of the Gasteiger type. A total of 256 docking trials for each ligand–protein combination were performed. Combinations with the lowest binding energy and the dominant conformation of the ligand in the 256 trials were two criteria that were used to cluster the ligand-docked structures. The *MGLtools* suite (http://mgltools.scripps.edu/) was used to analyze the docking results, which were subsequently visualized using *PyMOL*.

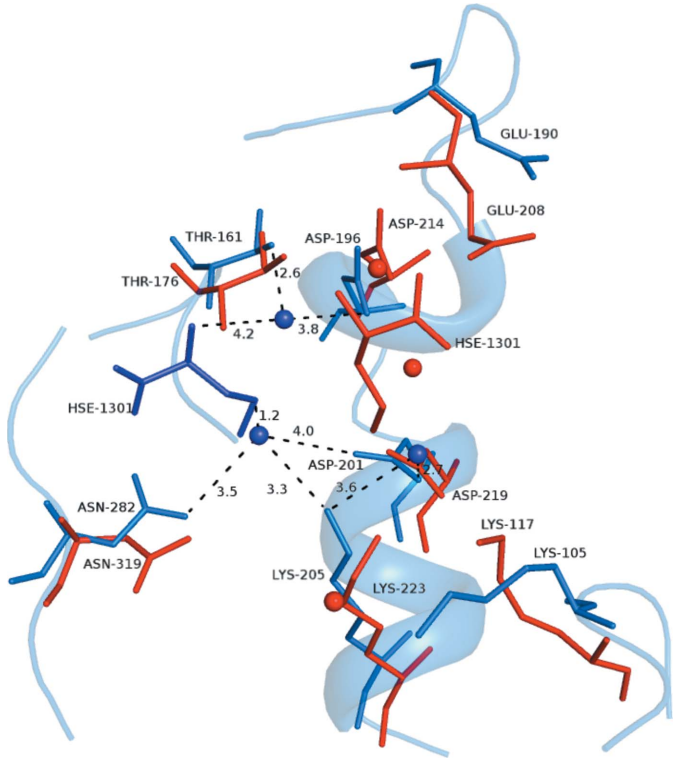

Figure 3
Comparison of the active site in *S. aureus* homoserine dehydrogenase (blue) with the *S. cerevisiae* homologue (red). The conserved structural features provided a basis to identify the substrate-binding residues and other residues crucial for catalytic activity (based on mutational analysis of the *S. cerevisiae* enzyme). The substrate L-Hse (blue) was docked into the active site of the *S. aureus* enzyme.

Table 3
Thermal shift assays to evaluate cofactor binding to *S. aureus* HSD.

Protein	T_m (°C)	T_m in the presence of 2 m*M* $NADP^+$ (°C)	Difference in the T_m (°C)
Native	47.7 ± 0.17	51.7 ± 0.05	4.0
K105A	48.0 ± 0.10	52.8 ± 0.04	4.8
K105R	48.3 ± 0.04	51.4 ± 0.05	3.1
K205A	48.3 ± 0.03	51.3 ± 0.04	3.0

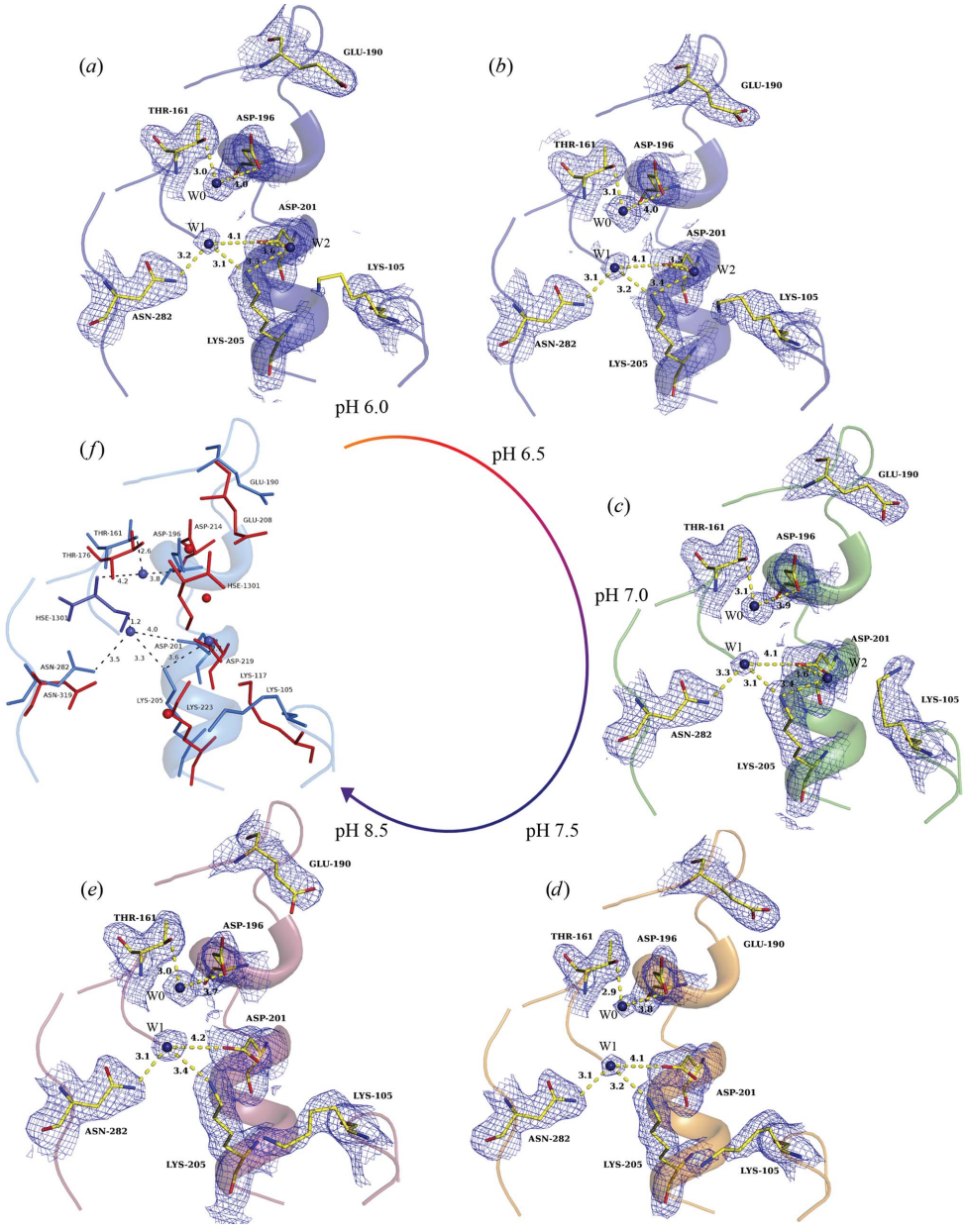

Figure 4
Variation in the hydration at the active site. The ($2mF_o - DF_c$) electron-density maps in this figure have been contoured at a similar (1σ) level. The resolution of the diffraction data at different pH conditions is broadly similar (~2.2 Å; Table 1). This figure represents chain *B* of *S. aureus* HSD. Snapshots of electron density at the active site are shown at increasing pH conditions (clockwise). The locations of the experimentally observed water molecules (blue) are shown at different pH conditions (*a*–*e*). The schematic of the reaction mechanism (involving the *gem*-diol form of ASA) is shown in an approximately similar orientation as the experimental maps and active-site model (*f*). Lys105 is seen to adopt different conformations at different pH conditions. Chain *A* of the *S. aureus* HSD dimer shows minimal hydration at all of the pH conditions (Supplementary Fig. S7).

2.8. Molecular-dynamics simulations

The HSD protein dimer was charged and 30 sodium ions were added to neutralize this effective charge. The simulations were run in the NPT ensemble. Pressure was maintained at 101.325 kPa using a Langevin piston and the temperature was set to 300 K. The H atoms were constrained to equilibrium positions and a time step of 2 fs was used to integrate the equations of motion. The simulation trajectories were analyzed using *Visual Molecular Dynamics* (*VMD*; Humphrey *et al.*, 1996). A generalized Born implicit solvent simulation of the unit cell of the crystal obtained at pH 7.5 was performed in the NVT ensemble to understand the effect of crystal packing on the refined temperature factors. The cutoff distances to compute the electrostatic interactions and the Born radius of each atom were set to 18 and 12 Å, respectively. The concentration of the ions was assumed to be 0.2 *M*. The H atoms were again constrained to equilibrium positions. A time step of 2 fs was used to advance the simulation, and the time period of the simulation trajectory for the unit cell was 10 ns.

3. Results and discussion

3.1. The structure of *S. aureus* HSD

The crystal structure of HSD was determined at 2.1 Å resolution. This enzyme is a dimer in solution as well as in the crystal (Fig. 2*a* and Supplementary Fig. S1). *S. aureus* HSD is an elongated molecule (with dimensions of ~80 × 45 × 20 Å) with three domains: a nucleotide cofactor-binding domain at the N-terminus, a central catalytic domain and a C-terminal ACT domain (Fig. 2*a*). The N-terminal domain of HSD is discontinuous, comprising of two segments [amino-acid residues 1–134 (β1–β6 and α1–α5) and 301–322 (α13)] separated by a catalytic domain (residues 135–300; β7–β11 and α6–α12). The C-terminal ACT domain adopts a character-

istic ferredoxin-like fold (β12–α14–β13–β14–α15–β15) and is connected to the α13 helix of the nucleotide cofactor-binding domain by a long loop (30 residues; Fig. 2*b*). This arrangement is similar to that in 3-phosphoglyceraldehyde dehydrogenase (3-PGDH), in which the nucleotide cofactor-binding domain is connected to the regulatory domain by a single long helix of ∼30 residues. This connecting helix contacts the substrate-binding region, thereby regulating the catalytic activity (Grant *et al.*, 2001).

The nucleotide cofactor-binding domain comprises of a six-stranded parallel β-sheet (β1–β6) surrounded by six helices (α1–α5 and α13) (Fig. 2*c*). The core of the domain contains a conserved phosphate-binding G*X*G*XX*G motif (comprising residues 10–15 located between β1 and α1), six conserved hydrophobic amino acids (Ile6, Leu8, Val19, Ile22, Ile29 and Leu33), a negatively charged amino acid (Asp36) at the C-terminus of β2 and a positively charged amino acid (Lys2) at the N-terminus of β1. In addition, a basic residue (Arg45) in the nucleotide cofactor-binding pocket stabilizes protein–cofactor interactions (Bellamacina, 1996; Lesk, 1995).

The catalytic domain comprises of a five-stranded anti-parallel β-sheet (β7–β11) with a α-helical cluster (α6–α12) at the periphery (Fig. 2*c*). The α-helical cluster contains the active site and the conserved homoserine dehydrogenase motif [A-x_3-G-(LIVMFY)-(STAG)-$x_{2,3}$-(DNS)-P-x_2-D-(LIVM)-x-G-x-D-x_3-K; residues 183–205]. The five β-strands from each monomeric unit form a rigid ten-stranded anti-parallel β-sheet that is crucial for the integrity of the dimer. The dimer interface is largely hydrophobic, with few polar interactions. Residues His252, Gln253 and Ala256 located on helix α12 and Met295, Phe296 and Tyr297 located on strand β11 contribute to dimerization (Fig. 2).

A comparison of *S. aureus* HSD (docked with substrate) with the other characterized homologue, *S. cerevisiae* HSD, revealed several similarities in the catalytic core (Fig. 3). The residues Lys117, Thr176, Glu208, Asp214, Asp219 and Lys223 in *S. cerevisiae* HSD were crucial for activity (DeLaBarre *et al.*, 2000). In the *S. aureus* enzyme Lys205 and Asp201 are the catalytic residues. Asp196, Glu190 and Thr161 play a role in substrate recruitment and positioning. Additionally, we note that a conserved residue, Asn282, interacts with a water molecule coordinated by Lys205 (Figs. 3 and 4). A structural comparison of the active sites across HSD structures also reveals that the conformations adopted by Thr161, Asn282, Asp201 and Lys205 are retained in the *S. aureus* enzyme. The only variation in the active site of *S. aureus* HSD is owing to the residues analogous to Glu190 and Asp196. This, in turn, results in a variation of the distance of Glu190 involved in substrate binding from the catalytic Lys205 (Fig. 3 and Supplementary Fig. S2).

3.2. Catalytic activity of HSD

The assay to determine the catalytic activity of HSD involved the detection of NADPH formation by measuring the absorption at 340 nm. A plot of specific activity *versus* temperature and pH yielded a bell-shaped curve irrespective of the substrate concentration (data not shown). Specific activity measurements were recorded at various pH conditions (pH 6.5–8.5) and temperatures (17, 27, 37 and 47°C). The catalytic activity of HSD was maximal at 37°C and pH 8.5. All enzyme assays were subsequently performed at basic pH (8.5) at 37°C (Supplementary Fig. S3). Enzyme assays were also performed in the presence of different metal ions (Zn^{2+}, Mg^{2+}, Na^+, K^+, Rb^+, Cs^+ and Li^+) as well as the plausible allosteric inhibitors L-threonine and L-serine. Unlike the *E. coli* and *S. cerevisiae* homologues, these metal ions did not significantly impact the activity of *S. aureus* HSD (Wedler *et al.*, 1992; Yumoto *et al.*, 1991). We also note that the kinetic behaviour of *S. aureus* HSD is not altered in the presence of plausible allosteric inhibitors such as L-threonine and L-serine (Supplementary Fig. S4). In this context, it is worth noting that these inhibitors could not be modelled in the experimental electron-density maps even in the cases of crystals grown in the presence of these inhibitors at high concentrations (Supplementary Table S2). The catalytic activity of two lysine mutants (the cofactor-binding Lys105 and the active-site Lys205) were also examined. The kinetic profiles of *S. aureus* HSD and the mutant enzymes are shown in Fig. 5 and Supplementary Fig. S3.

3.3. Structural basis for the catalytic mechanism

The reaction catalyzed by HSD relies on conserved water molecules at the active site. The experimental electron-density maps of *S. aureus* HSD were thus examined for structured waters at the active site at different pH conditions. Preliminary observations of the crystal structures of *S. aureus* HSD at different pH conditions revealed that one chain (chain *B*) has significantly higher thermal factors than the other (Supplementary Fig. S5). This finding was evaluated using MD simulations. In terms of the packing of *S. aureus* HSD in the crystal, each unit cell contains four protein dimers. A dimer in the centre is surrounded by three other dimers in the unit cell.

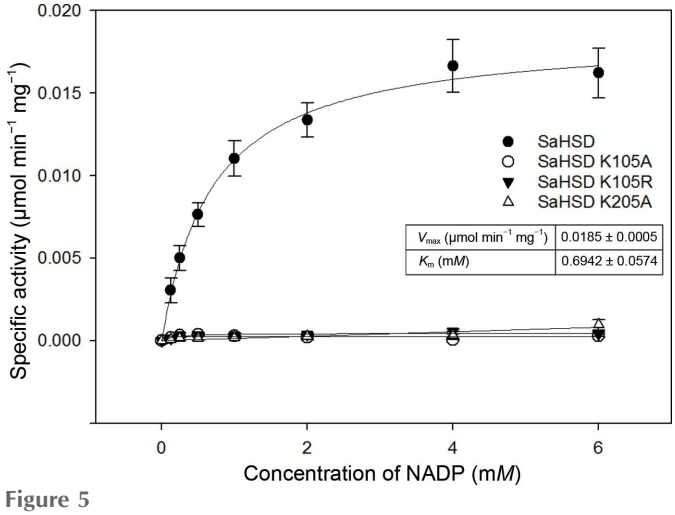

Figure 5
Catalytic activity of HSD. The K205A (unfilled triangles), K105A (unfilled circles) and K105R (filled triangles) mutations render *S. aureus* HSD (filled circles) inactive. The kinetic parameters are presented in the inset.

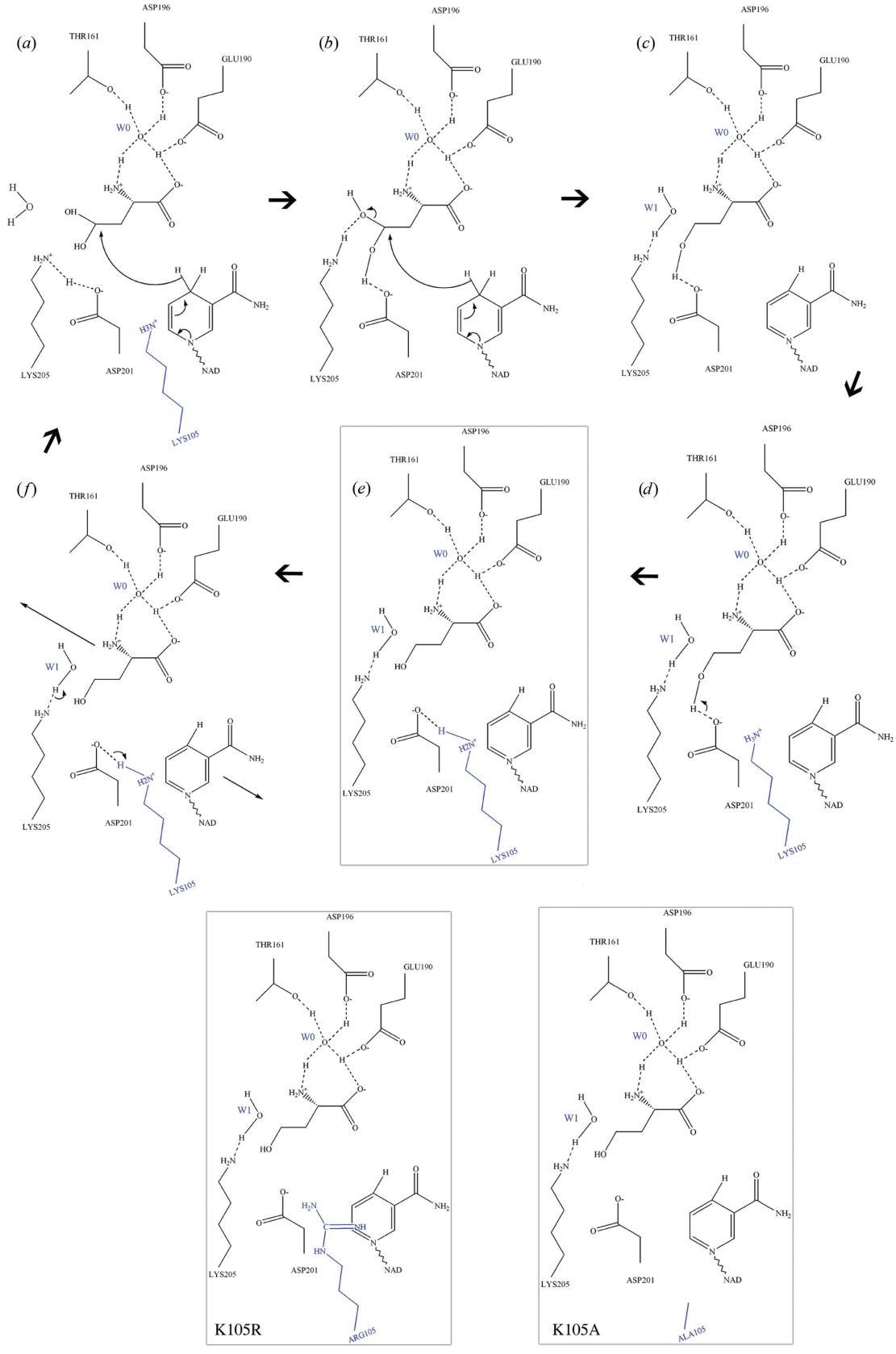

Figure 6
Mechanistic events at the active site. Asp196 and Glu190 are involved in substrate recruitment. Asn282 and Thr161, along with Asp201, help in substrate positioning. This is independent of the aldehyde or *gem*-diol form adopted by ASA (described in Fig. 1). Lys205 acts as a general acid in the catalysis (DeLaBarre *et al.*, 2000). Lys105 stabilizes Asp201 and aids in release of the product from the active site. (*a*)–(*f*) represent various steps of catalysis. The effect of mutation of Lys105 to Arg or Ala is highlighted.

The root-mean-square fluctuation (r.m.s.f.) of the C^{α} atoms in the dimer present at the centre of the unit cell were calculated to evaluate the role of crystal packing on the *B* factors of the two protein segments present in the dimer. The last 5 ns of the 10 ns trajectory were used to calculate the r.m.s.f.. Before calculating the r.m.s.f., all of the conformations of the central protein dimer in the unit cell were aligned with the PDB structure. The r.m.s.f. calculated with respect to the PDB structure is represented in Supplementary Fig. S6. This analysis led us to conclude that the apparent flexibility of one monomeric chain is an artifact of crystal packing. The subsequent discussion on hydration dynamics is thus limited to chain *B*, and the equivalent features in chain *A* are shown in Supplementary Fig. S7.

A change in the pH results in substantial changes in the hydrogen-bonding network between Thr161, Asp201, Lys205 and Asn282 (Fig. 4). Asp201 and Lys205 coordinate a water molecule (W2) at acidic pH (at pH 6.0, 6.5 and 7.0), which is displaced as the pH is increased to 7.5. At basic pH (7.5 and 8.5) only two water molecules are retained at the active site, one (W0) bound to Thr161 and the other (W1) between Lys205 and Asn282. These two waters provide a template to rationalize the catalytic mechanism. The role of water W0 coordinated to Thr161 (equivalent to Thr176 in *S. cerevisiae* HSD) has been described earlier (DeLaBarre *et al.*, 2000). The focus of this analysis was thus on the role of the water molecule W1 coordinated between Asn282 and the active-site lysine Lys205.

Two putative reaction mechanisms rationalize the forward reaction of HSD. One favours the aldehyde form, while the other favours the *gem*-diol form of ASA as the substrate. The reverse reaction adopts the *gem*-diol form of ASA. In this step, L-Hse is positioned closer to the catalytic aspartate residue (Asp219 in *S. cerevisiae* and Asp201 in *S. aureus*) such that the C^{γ}–OH of the substrate faces the catalytic lysine (Lys223 in *S. cerevisiae* and Lys205 in *S. aureus* HSD) that is hydrated. In the crystal structure of the *S. cerevisiae* HSD–L-Hse complex, L-Hse is closer to Asp219 than Lys223 (Fig. 3).

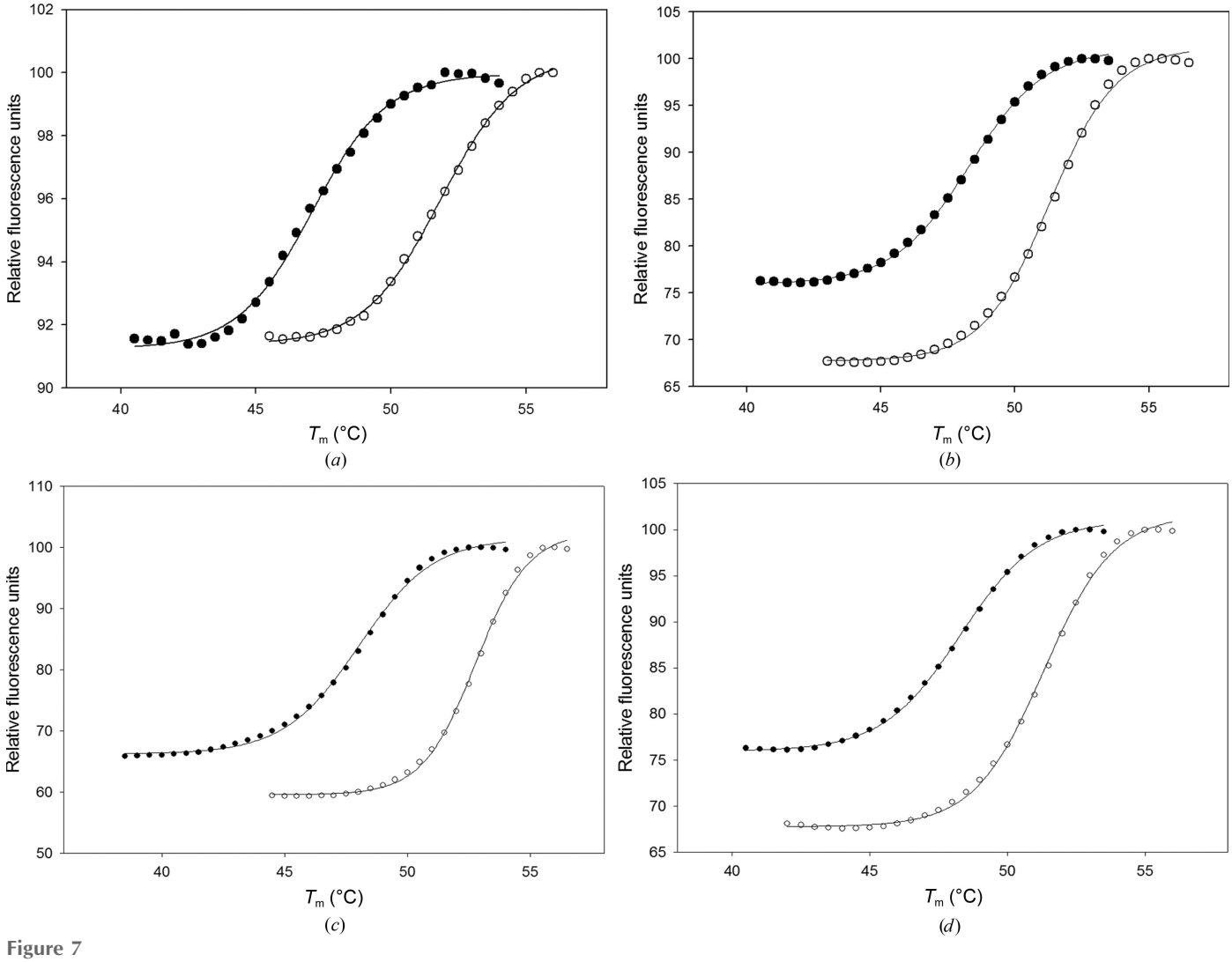

Figure 7
Thermal shift assay. In thermal shift assays to evaluate NADP binding, *S. aureus* HSD and its mutants showed a similar increase in thermostability in the presence of the cofactor. (*a*) *S. aureus* HSD (filled circles) and in the presence of cofactor (unfilled circles). (*b*) Lys205Ala mutant HSD. (*c*) Lys105Ala mutant HSD. (*d*) Lys105Arg mutant HSD.

It was suggested that this conformation would allow Lys223 to coordinate a water molecule. The active site of *S. aureus* HSD provides experimental confirmation of this hypothesis. A water molecule coordinated by Lys205 and Asn282 is present in all of the pH conditions that were examined (pH 6.0–8.5; Fig. 4). Indeed, replacing Lys205 with Ala rendered the protein inactive (Fig. 5). Lys205 abstracts a proton from the coordinated water, generating a hydroxyl group which can attack the C4 position of L-Hse, giving rise to the *gem*-diol form of ASA (Fig. 1). The forward reaction involving the *gem*-diol form would mirror this step, in which the hydroxyl group of ASA is displaced as a water molecule, generating L-Hse. In this reaction, the two hydroxyl groups of the *gem*-diol form of ASA make hydrogen bonds to Lys205 (referred to as the departing hydroxyl group) and Asp201 (also called the remaining hydroxyl group). In this reaction, the departing hydroxyl group accepts a proton from Lys205. A hydride from the cofactor attacks the C4 atom of the substrate, resulting in the release of the departing hydroxyl group as water (DeLaBarre *et al.*, 2000). The remaining hydroxyl group is held by a hydrogen bond to the carboxylate group of Asp201. As Lys205 is bound to the released water molecule, Lys105 stabilizes Asp201, thereby releasing the product (a protonated alcohol; Fig. 6).

In *S. cerevisiae* HSD it was observed that a residue equivalent to Lys105 (Lys117 in the *S. cerevisiae* enzyme) plays a crucial role in catalysis by aiding in positioning the cofactor. Lys117 is located in a 3_{10}-helix (α-1F) and the position of this helix alters only slightly upon cofactor binding. Mutation of this residue led to inactivation of the *S. cerevisiae* enzyme. In *S. aureus* HSD Lys105 is located in a loop present between the catalytic site and the cofactor-binding site. This confers greater flexibility to Lys105, thus enabling interactions with either Asp201 of the catalytic site or the bound cofactor. It thus appears likely that Lys105 in *S. aureus* HSD acts to stabilize Asp201 and to aid in the product-release step of the reaction mechanism. It is worth noting in this context that while substitution of Lys105 by Arg or Ala rendered the protein inactive, this was not owing to defective cofactor binding (Figs. 5, 6 and 7). The thermal shift assays performed with the mutant enzymes (both K105A and K105R HSD) suggest that the mutations did not have altered cofactor binding (Fig. 7 and Table 3).

Put together, the crystal structure and mutational analysis suggest a crucial role for Lys105 in the catalytic mechanism of *S. aureus* HSD. This residue, located at the interface between the catalytic and cofactor-binding domains, governs hydride transfer from the catalytic site to the cofactor-binding site. An analysis of the crystal structures at different pH conditions suggests that hydration dynamics and water diffusion at the active sites govern distinct steps in the reaction catalyzed by *S. aureus* HSD.

Acknowledgements

The macromolecular crystallography facility at the Molecular Biophysics Unit is supported by grants from the Department of Science and Technology, Government of India. We acknowledge Dr Hassan Belrhali and Dr Babu A. Manjasetty for their help in data collection at beamline BM14 of the European Synchrotron Radiation Facility (ESRF), Grenoble.

References

Aravind, L. & Koonin, E. V. (1999). *J. Mol. Biol.* **287**, 1023–1040.
Archer, J. A., Solow-Cordero, D. E. & Sinskey, A. J. (1991). *Gene*, **107**, 53–59.
Battye, T. G. G., Kontogiannis, L., Johnson, O., Powell, H. R. & Leslie, A. G. W. (2011). *Acta Cryst.* D**67**, 271–281.
Bellamacina, C. R. (1996). *FASEB J.* **10**, 1257–1269.
Cowtan, K. (2006). *Acta Cryst.* D**62**, 1002–1011.
Cremer, J., Treptow, C., Eggeling, L. & Sahm, H. (1988). *J. Gen. Microbiol.* **134**, 3221–3229.
Curien, G., Biou, V., Mas-Droux, C., Robert-Genthon, M., Ferrer, J.-L. & Dumas, R. (2008). *Plant Physiol. Biochem.* **46**, 325–339.
DeLaBarre, B., Thompson, P. R., Wright, G. D. & Berghuis, A. M. (2000). *Nature Struct. Biol.* **7**, 238–244.
Emsley, P. & Cowtan, K. (2004). *Acta Cryst.* D**60**, 2126–2132.
Grant, G. A., Hu, Z. & Xu, X. L. (2001). *J. Biol. Chem.* **276**, 17844–17850.
Humphrey, W., Dalke, A. & Schulten, K. (1996). *J. Mol. Graph.* **14**, 33–38.
Jacques, S. L., Ejim, L. J. & Wright, G. D. (2001). *Biochim. Biophys. Acta*, **1544**, 42–54.
Jacques, S. L., Nieman, C., Bareich, D., Broadhead, G., Kinach, R., Honek, J. F. & Wright, G. D. (2001). *Biochim. Biophys. Acta*, **1544**, 28–41.
Lesk, A. M. (1995). *Curr. Opin. Struct. Biol.* **5**, 775–783.
McCoy, A. J., Grosse-Kunstleve, R. W., Adams, P. D., Winn, M. D., Storoni, L. C. & Read, R. J. (2007). *J. Appl. Cryst.* **40**, 658–674.
Morris, G. M., Huey, R., Lindstrom, W., Sanner, M. F., Belew, R. K., Goodsell, D. S. & Olson, A. J. (2009). *J. Comput. Chem.* **30**, 2785–2791.
Murshudov, G. N., Skubák, P., Lebedev, A. A., Pannu, N. S., Steiner, R. A., Nicholls, R. A., Winn, M. D., Long, F. & Vagin, A. A. (2011). *Acta Cryst.* D**67**, 355–367.
Navratna, V. & Gopal, B. (2013). *Acta Cryst.* F**69**, 1216–1219.
Painter, J. & Merritt, E. A. (2006). *Acta Cryst.* D**62**, 439–450.
Parsot, C. & Cohen, G. N. (1988). *J. Biol. Chem.* **263**, 14654–14660.
Reinscheid, D. J., Eikmanns, B. J. & Sahm, H. (1991). *J. Bacteriol.* **173**, 3228–3230.
Schroeder, A. C., Zhu, C., Yanamadala, S. R., Cahoon, R. E., Arkus, K. A., Wachsstock, L., Bleeke, J., Krishnan, H. B. & Jez, J. M. (2010). *J. Biol. Chem.* **285**, 827–834.
Thomas, D., Barbey, R. & Surdin-Kerjan, Y. (1993). *FEBS Lett.* **323**, 289–293.
Truffa-bachi, P., Veron, M., Cohen, G. N. & Stadtman, E. R. (1974). *Crit. Rev. Biochem. Mol. Biol.* **2**, 379–415.
Wedler, F. C., Ley, B. W., Shames, S. L., Rembish, S. J. & Kushmaul, D. L. (1992). *Biochim. Biophys. Acta*, **1119**, 247–249.
Winn, M. D. *et al.* (2011). *Acta Cryst.* D**67**, 235–242.
Yumoto, N., Kawata, Y., Noda, S. & Tokushige, M. (1991). *Arch. Biochem. Biophys.* **285**, 270–275.